RSC Advances

ROYAL SOCIETY OF CHEMISTRY

www.rsc.org/advances

Regio- and Diastereoselectivity of the 1,3-Dipolar Cycloaddition of α-aryl Nitrone with Methacrolein. A Theoretical Investigation

Wafaa Benchouk and Sidi Mohamed Mekelleche*

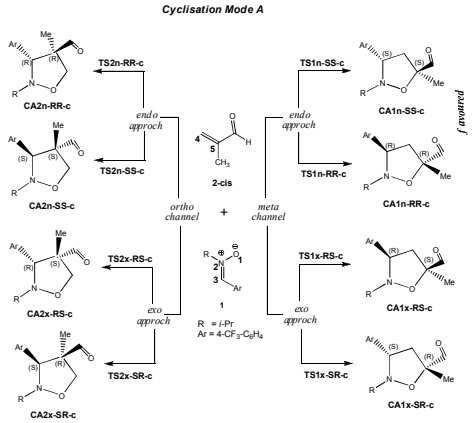

Regio- and Diastereoselectivity of the 1,3-Dipolar Cycloaddition of α-aryl Nitrone with Methacrolein. A Theoretical Investigation

Wafaa Benchouk and Sidi Mohamed Mekelleche*

Laboratory of Applied Thermodynamics and Molecular Modelling, Department of Chemistry, Faculty of Science, University of Tlemcen, PB 119, Tlemcen, 13000, Algeria.

Corresponding author:
sm_mekelleche@mail.univ-tlemcen.dz (S. M. Mekelleche)

The mechanism, regio- and diastereoselectivity of the 1,3-dipolar cycloaddition of *N*-*iso*-propyl,*α*-(4-trifluoromethyl)-phenyl nitrone with methacrolein yielding the isoxazolidine cycloadduct [V. Bãdoiu, E. P. Kündig, *Org. Biomol. Chem.*, 2012, **10**, 114] has been studied at the B3LYP/6-31G(d) level of theory. The two conformations *s*-*cis* and *s*-*trans* of methacrolein are considered in the cyclisation modes and all the possible regio-(*ortho*/*meta*) and stereo-(*endo*/*exo*) isomeric channels to provide the different diastereoisomers were thoroughly investigated. The free activation enthalpies, calculated with the MPW1B95/6-31G(d) method, in dichloromethane show that the *meta*-*endo* channel corresponding to the cyclisation mode between the nitrone and the *s*-*cis* methacrolein giving the RR/SS diastereoisomers is the most favoured reaction channel as expected experimentally. Intrinsic reaction coordinate (IRC) calculations and the topological analysis of the electron localization function (ELF) of some relevant points of the IRC curve show that the *meta*-*endo* favoured channel takes place via a one-step non-concerted mechanism. Charge transfer calculations performed at the transition states in combination with the calculation of DFT-based reactivity indices of the reactants reveal a low polar character of the studied reaction.

Keywords: 1,3-Dipolar Cycloaddition; Nitrones; Isoxazolidine; Regioselectivity; Diastereoselectivity; Density functional theory.

Introduction

The synthetic utility of the 1,3-dipolar cycloaddition (13DC) reaction is evident from the number and scope of targets that can be prepared by this chemistry.[1] As one of the most thoroughly investigated 1,3-dipoles, nitrones have been successfully employed to generate nitrogen- and oxygen-based functionality from the cycloadducts as well as the potential to introduce of new and multiple chiral centers stereoselectively.[1]

The most common 13DC reaction of nitrones is the formation of an isoxazolidine using alkene dipolarophiles (see Scheme 1), although other multiply bonded systems may also be used (alkynes, allenes, isocyanates, nitriles, thiocarbonyls, etc.). Isoxazolidines compounds have attracted interest as a result of biological activity, including anti-HIV and cytotoxicity, resulting from their ability to act as nucleoside analogs.[2] In addition, they have served as synthetic precursors to other classes of natural products, such as 1,3-amino alcohols, β-lactams, and alkaloids with physiological activity.[3] The isoxazolidine cycloadduct contains up to three new chiral centers (see scheme 1) and, as with other 1,3-dipoles, the highly ordered transition state often allows the regio- and stereochemical preference of a given nitrone to be predicted.[1,4] This prediction is achieved through a consideration of steric and electronic factors.

The 13DC reaction of nitrones with dipolarophiles can produce both *endo* and *exo* isoxazolidine cycloadducts;[5] this nomenclature is well-known from the Diels-Alder (DA) reaction.[6] If the dipolarophile, or the 1,3-dipole, contains chiral center(s), the approach toward one of the faces of the 1,3-dipole or dipolarophile can be discriminated, leading to a diastereoselective reaction. The term enantioselectivity will only be applied when optically active products are obtained from achiral or racemic starting materials.[5] The selectivity in the 13DC reaction is therefore primarily controlled by the structure of the substrates or by application of chiral Lewis acids (LAs). In this context, the use of metal-based catalysts, organo-catalysts in modern 13DC asymmetric organic synthesis have been expanding uninterruptedly during the last decades.[7] Several experimental studies on the regio-, enantio- and *endo/exo* diastereoselective synthesis of 13DC reactions of nitrones can be found in the literature.[8] Nitrones bearing various substituents at the nitrogen atom of the nitrone were synthesized by Bădoiu et al.[9] in order to expand the range of transformations that can be carried out on the isoxazolidine core following the 13DC reaction. In this series, the *N*-*i*-Pr

(see Scheme 2) and -*t*-Bu nitrones, respectively, gave the products in moderate yields despite long reaction times and a two-fold excess of methacrolein.

Several experimental works supported by theoretical approaches to investigate the regio-, stereo- and diastereoselectivity of the 13DC of nitrones can be found in the literature.[10-13] The regioselectivity and *endo*/*exo* selectivities of the 13DC reaction of 1-pyrroline-1-oxide to methyl cinnamate and benzylidene acetophenone were rationalized through both experimental and theoretical findings by Acharjee et al..[11] Flores et al.[12] undertook a theoretical study of 13DCs of phenylvinylsulfone and several nitrones in order to explain the experimental results, including the regiochemistry, diastereoselectivity, and kinetic control. The reaction mechanism of the 13DC of C,N-diphenylnitrone with unsaturated valerolactone under thermal and LA-mediated conditions has been studied by Śnieżek et al.[13] using DFT and MP3 methods. Benchouk et al.[14] studied the role of LA catalysts on the 13DC of N-benzylideneaniline N-oxide nitrone with acrolein using DFT calculations. The regioselectivity of the 13DC of C-(methoxycarbonyl)-N-methyl nitrone with methyl acrylate and vinyl acetate have been analysed by Merino et al.[10b] and Benchouk et al.[15] using several theoretical approaches.

In the present work, we present a theoretical study of the regio-, stereo- and diastereoselectivity of the non-catalyzed 13DC of *N*-*iso*-propyl, *α*-(4-trifluoromethyl)-phenyl nitrone **1** and methacrolein **2**, experimentally studied by Bãdoiu et al.[9] (see Scheme 2). We note that the best yields of diastereoselectivities (in favour of the *endo* isomer) have been obtained in the case of non-catalyzed reaction (in comparison of the catalyzed one) using the *N*-*i*-Pr and *t*-Bu nitrones and exclusively the 3,5-substituted regioisomers were isolated (see Scheme 2).[9] Firstly, in order to justify the most favoured cyclisation approach, we have performed a density functional theory (DFT) study with the aim to localize the stationary points for reactants, transition structures (TSs), cycloadducts (CAs) of all the possible regio- and stereoisomeric channels on the potential energy surface (PES). Then, the reaction mechanism is discussed and analysed on the basis of the intrinsic reaction coordinate (IRC) calculations and the topological analysis of the electron localization function (ELF). Finally, a complementary study based on reactivity indexes defined within the conceptual DFT is used to analyze the polar (vs. non polar) character of the studied 13DC reaction.

Results and discussion

The α-aryl nitrone **1** exists in both *Z* and *E* conformations. B3LYP/6-31G(d) calculations show that the *Z* conformation is more stable than the *E* conformation by 7.9 kcal/mol (see S2-S3 of the Electronic supplementary information ESI). This finding is in accordance with experimental outcome since ^{1}H NMR analysis at room temperature showed that only the *Z* isomer present in solution.[9] For this reason, only the *Z* conformation of the α-aryl nitrone **1** will be considered in the 13DC reaction under study. Liu et al.[16] performed theoretical and experimental analyses of the conformational switches in TSs of some DA and 13DC cycloadditions. Barba et al.[17] showed that the preference of the *s-cis*/*s-trans* conformation of methacrolein **2** in DA and 13DC cycloadditions derives from a delicate balance between the larger stability of the *s-trans* conformer of the ground-state of methacrolein and the larger reactivity of the corresponding *s-cis* conformation. B3LYP/6-31G(d) calculations show that the *s-trans* conformation of methacrolein **2-trans** is lower in energy than the **2-cis** conformation by 2.9 kcal/mol (see S4 of the ESI). Both the *s-cis* and *s-trans* conformations of methacrolein (see Schemes 3-4) have been considered in the present study.

In the present theoretical study of the regio- and diastereoselectivity of the 13DC reaction, two cyclisation modes were investigated. The cyclisation mode A (**CM-A**) corresponding to the 13DC reaction between α-aryl nitrone **1** with methacrolein **2-cis** (Scheme 3) and the cyclisation mode B (**CM-B**) corresponding to the 13DC reaction between α-aryl nitrone **1** with methacrolein **2-trans** (Scheme 4). Due to the asymmetry of the dipole and the dipolarophile, in the 13DC reaction of the α-aryl nitrone **1** with methacrolein **2-cis/trans**, several reaction channels are feasible. The formation of eight isomeric isoxazolidines cycloadducts for **CM-A** and eight isomeric isoxazolidines cycloadducts for **CM-B** can be related to the two regioisometric channels *ortho* and *meta* and the two stereoisomeric approaches *endo* and *exo* (Schemes 3-4). The experimental findings due to Bãdoiu et al.[9] indicate that this cycloaddition reaction is characterized by a complete *endo* stereoselectivity with the unique formation of the regioisomer associated with the formation of the O1–C5 and C3–C4 sigma bonds (Schemes 3-4). Bãdoiu and co-workers have also found, for this non-catalyzed reaction, that the enantioselectivity is moderate and a racemic mixture of the (3R,5R) and (3S,5S) enantiomers was obtained. In order to explain the origin

of the regio- and diastereoselectivity experimentally observed, sixteen reaction channels were investigated and analysed (Schemes 3-4). In this study, we have considered the two regioisomeric channels, namely *ortho* and *meta*, corresponding to the formation of the 3,4 and 3,5-disubstituted isoxazolidines, respectively. We note that the regioselectivity is referred to the attack of the oxygen atom of the α-aryl nitrone **1** to the carbon atom of the C-C double bond of methacrolein. Due to the mutual orientation of reactants, two stereoisomeric approaches can be considered, namely, *endo* and *exo*, corresponding to the position of the carbonyl group of methacrolein **2** towards to the nitrogen atom of α-aryl nitrone **1**. The presence of the four possible diastereoisomeric cycloadducts identified in the reaction is fully justified by the existence of two chiral centers for each regioisomer. Consequently, a total of sixteen reaction channels have been investigated. Eight TSs for **CM-A**, namely, **TS1n-SS-c**, **TS1n-RR-c**, **TS1x-RS-c**, **TS1x-SR-c**, **TS2n-RR-c**, **TS2n-SS-c**, **TS2x-RS-c** and **TS2x-SR-c** and the corresponding isoxazolidines cycloadducts **CA1n-SS-c**, **CA1n-RR-c**, **CA1x-RS-c**, **CA1x-SR-c**, **CA2n-RR-c**, **CA2n-SS-c**, **CA2x-RS-c** and **CA2x-SR-c** (see Scheme 3 and pages S5-S20 of the ESI) and eight TSs for **CM-B**, namely, **TS1n-SS-t**, **TS1n-RR-t**, **TS1x-RS-t**, **TS1x-SR-t**, **TS2n-RR-t**, **TS2n-SS-t**, **TS2x-RS-t** and **TS2x-SR-t** and the corresponding isoxazolidines cycloadducts **CA1n-SS-t**, **CA1n-RR-t**, **CA1x-RS-t**, **CA1x-SR-t**, **CA2n-RR-t**, **CA2n-SS-t**, **CA2x-RS-t** and **CA2x-SR-t** (see Scheme 4 and pages S21-S36 of the ESI) were located and characterized on the PES. The calculated energies of all the stationary points in gas phase and in dichloromethane (DCM) are summarized in Table 1. It turns out the most favourable reaction pathway corresponds to the formation of the *endo* stereoisomeric isoxazolidines cycloadducts **CA1n-SS-c** and **CA1n-RR-c** enantiomers, via **TS1n-SS-c** and **TS1n-RR-c**, respectively. We note that for the **CM-A**, the **TS1n-SS-c** and **TS1n-RR-c** TSs are located 15.4 kcal/mol above the reagents in the gas phase. The energy differences between **TS1n-SS-c/TS1n-RR-c** and the other couples of enantiomers are 5.9 kcal/mol for **TS1x-RS-c/ TS1x-SR-c**, 1.2 kcal/mol for **TS2n-SS-c/ TS2n-RR-c** and 7.2 kcal/mol for **TS2x-RSc/TS2x-SR-c**. For the **CM-B**, the most favourable reaction pathway corresponds to the formation of the *endo* **CA1n-SS-t** and **CA1n-RR-t** cycloadducts, via **TS1n-SS-t** and **TS1n-RR-t**, respectively. Indeed, the **TS1n-SS-t** and **TS1n-RR-t** TSs are located 20.2 kcal/mol above the reagents in the gas phase. The energy difference between **TS1n-SS-t/TS1n-RR-t** and the other couples of enantiomers are 2.6 kcal/mol for **TS1x-RS-t/TS1x-SR-t**, 1.7 kcal/mol for **TS2n-SS-t/TS2n-RR-t** and 3.6 kcal/mol for **TS2x-RS-t/TS2x-SR-t**. It turns out

that the **CM-A** is more favoured than **CM-B**. Indeed, the **TS1n-SS-c/TS1n-RR-c** are lower in energy than **TS1n-SS-t/TS1n-RR-t** by 4.8 kcal/mol, indicating a clear preference of the *meta-endo* reaction channel via **CM-A** which is in agreement with experimental findings.[9]

Solvent effects on cycloaddition reactions are well-known and they have received considerable attention.[1,18-19] With the inclusion of solvent effects (see Table 1), the TSs and CAs are more stabilized than reactants and the *meta-endo* reaction channel via **CM-A** is still the favoured one although the activation energy associated with **TS1n-SS-c/TS1n-RR-c** is increased from 15.4 kcal/mol (in gas phase) to 18.2 kcal/mol (in DCM).

It is well-recognized that the B3LYP DFT functional is not adequate for thermochemical calculations and the MPW1PW91/6-311+G(d,p) and MPW1B95/6-31(d) computational levels were found to give a reasonably good agreement with the experimental kinetics and thermodynamic parameters for chemical reactions.[20,21] The relative Gibbs free energies in DCM for the sixteen reaction channels were computed at the MPW1B95/6-31(d) level of theory using B3LYP/6-31G(d) optimized geometries and the obtained results are summarized in Table 2. The analyses of the tabulated results show that the *meta-endo* reaction channel via **CM-A** yielding to the formation of the **CA1n-SS-c/CA1n-RR-c** isomers is favoured both kinetically and thermodynamically. We note that this favoured reaction channel is remarkably exothermic by 19.5 kcal/mol.

The geometries of the eight TSs (four for **CM-A** and four for **CM-B**) prepared using CYLView,[22] are given in Figure 1. Obviously, for each couple of enantiomers, the bond lengths for the two forming sigma bonds are identical. The extent of bond formation along a reaction pathway is provided by the concept of bond order (BO).[23] At the TSs associated to the *meta-endo* reaction channel via **CM-A**, the BO values of the two forming bonds are: 0.21 (O1–C5) and 0.48 (C3–C4) for **TS1n-SS-c/TS1n-RR-c**, 0.25 (O1–C5) and 0.48 (C3–C4) for **TS1x-RS-c/TS1x-SR-c** indicating that the C3–C4 sigma bond is more advanced than the O1–C5 sigma bond. By contrast, at the TSs associated to the *ortho-endo* reaction channel via **CM-A**, the BO values of the two forming bonds are: 0.60 (O1–C4) and 0.22 (C3–C5) for **TS2n-SS-c/TS2n-RR-c**, 0.57 (O1–C4) and 0.25 (C3–C5) for **TS2x-RS-c/TS2x-SR-c** indicating that the O1–C4 sigma bond is more advanced than C3–C5 sigma bond. On the

other hand, it is well known that when a 13DC cycloaddition presents highly asynchronous TSs, diradical structures could in principle be involved. The stability test for equilibrium geometries of the transition state **TS1n-SS-c** of the asynchronous mechanism was performed using the "STABLE" Gaussian keyword. The output indicates that "*The wave function is stable under the perturbations considered*". Consequently, we can conclude the inexistence of diradical TS structures.

IRC calculations indicate that the 13DC cycloaddition of α-aryl nitrone **1** with methacrolein **2-cis** follows a one-step mechanism and the eventuality of a stepwise mechanism is excluded. Indeed, the optimization of the last structure on the IRC curve in the forward direction gives a structure identical to that of the cycloadduct, indicating the absence of a stable reaction intermediate. Topological analysis of the ELF along the reaction pathway in 13DC and DA cycloaddition[21b,24] can be also used as a valuable tool to understand the bonding changes along the reaction channel. Silvi[25] proposed the topological approach of the chemical bonding which enables a position space partition of the electron density in terms of basins of attractor whose chemical significance is given by their location with respect to the nuclei. Indeed, there are two types of basins: core and valence. Core basins correspond to the inner atomic shell density while valence basin density is organized around and between the core basins. The latter are characterized by the number of core basin with which they have a boundary; this number is called the *synaptic order*. There are therefore monosynaptic basins corresponding to electron lone pairs or non-bonding regions, labeled V(A), while disynaptic basins to conventional two-center bonds, connect the core of two nuclei A and B and, thus, correspond to a bonding region between A and B and are labeled as V(A,B). These graphical representations of molecules in terms of localization domains are very helpful since they provide a direct access to the chemical understanding. In order to explain the bond formation in this 13DC reaction, a topological analysis of the ELF of some relevant points of the IRC curve (forward direction) of the most favorable *meta-endo* reaction channel via **CM-A** associated with the reaction between the α-aryl nitrone **1** and methacrolein **2-cis** was performed. The ELF valence basins and their corresponding N populations of the relevant points **TS1n-SS-c**, **P-I**, **P-II, P-III, PIV** and **CA1n-SS-c** are given in Table 3. The schematic representation of the mono- and disynaptic basins for the five considered points is given in Figure 2 and the cartesian coordinates of the structures corresponding to **P-I**, **P-II, P-III** and

P-IV are given in pages S37-S40 of the ESI. Interesting conclusions can be drawn from the ELF analysis: (i) the presence of two monosynaptic basins, V(C3) and V(C4), integrating 0.63e and 0.34e, respectively at the **TS1n-SS-c**. (ii) a disynaptic basin V(C3,C4), N=1.58e is formed after the TS and it corresponds to the first new C3–C4 sigma bond (**P-I**). (iii) the presence of new V(C5) monosynaptic basins, integrating 0.26e is observed at **P-II**. (iv) a disynaptic basin V(O1,C5), N=0.92e, is formed in a late stage (**P-III**). (v) the two disynaptic basins associated with two single bonds formed in this 13DC reaction have reached an electron density of 1.83e (C1-C6) and 1.09e (O1-C5) at the **P-IV** just before the formation of the cycloadduct **CA1n-SS-c**. Consequently, the studied 13DC reaction, involving asymmetric reagents, occurs via a one-step non-concerted mechanism.

Another important aspect of cycloaddition reactions is the analysis of the polarity of the process. The natural population analysis (NPA) is a suitable tool to evaluate the charge transfer (CT) at the TSs. The natural charges at the TSs were shared between the α-aryl nitrone **1** and methacrolein **2-cis**. The calculations show that the electron flux takes place from **1** to **2-cis** for all the eight TSs for *meta-endo* reaction channel via **CM-A** and the CT values are as follows: 0.07e at **TS1n-SS-c/TS1n-RR-c**, 0.05e at **TS1x-RS-c/TS1x-SR-c**, 0.11e at **TS2n-RR-c/TS2n-SS-c**, 0.09e at **TS2x-RS-c/TS2x-SR-c**. These negligible CTs point out to a low polar cycloaddition process. These findings were confirmed by the calculation of DFT-based reactivity indices of the isolated reagents. In Table 4, we reported the energies of the frontier molecular orbitals HOMO, ε_H, and LUMO, ε_L, and the global properties (electronic chemical potential, μ, chemical hardness, η, Parr's electrophilicity index, ω) of the α-aryl nitrone **1** and methacrolein **2-cis**. The electrophilicity index of the α-aryl nitrone **1**, ω=1.70 eV, allows to classify this species as a strong electrophile within the electrophilicity scale.[26] This value is slightly lower than that of methacrolein **2-cis**, ω=1.75 eV. The very low electrophilicity difference, Δω=0.05 eV, between the two reactants puts in evidence the very low polar character of the 13DC reaction under study. In conclusion, for the favoured *meta-endo* reaction channel via **CM-A**, the relatively high activation energy in solution, 18.2 kcal/mol, explains the experimental findings, indicating that the studied 13DC reaction occurs at room temperature. We note that 13DC reactions with activation barriers of about 5-8 kcal/mol are known to take place at low temperatures.

Conclusion

In the present work, the mechanism, regio- and diastereoselectivity of the 13DC of the α-aryl nitrone **1** and methacrolein **2-cis/trans** to yield the isoxazolidine cycloadduct have been studied at the B3LYP/6-31G(d) level of theory. The sixteen reaction channels associated to different cyclisation modes of the reagents have been thoroughly elaborated and analysed. DFT calculations performed both in gas phase and in DCM, show that the *meta-endo* reaction channel via **CM-A,** yielding the (3R, 5R) and (3S, 5S) *endo* cycloadducts, is favoured both kinetically and thermodynamically. These results are in good agreement with experimental findings. The IRC calculations combined to ELF analysis show that the studied 13DC reaction follows a one-step non-concerted mechanism. The relatively high activation energy for the favoured *meta-endo* reaction channel via **CM-A** explains the fact that this reaction takes place at room temperature and it is not favoured at low temperatures. The low CT at **TS1n-SS-c** and the low electrophilicity difference between the reagents **1** and **2-cis** explain the low polarity of the studied 13DC reaction.

Computational methods

All calculations were carried out with the Gaussian 09 suite of programs.[27] DFT calculations were performed using Becke's three-parameter hybrid exchange functional in combination with the gradient corrected correlation functional of Lee et al. (B3LYP)[28] together with the standard 6-31G(d) basis set.[29] The optimizations were carried out using the Berny analytical gradient optimization method.[30] The stationary points were characterized by frequency calculations in order to verify that TSs had one and only one imaginary frequency. The IRC path[31] was traced in order to check the energy profiles connecting each TS to the two associated minima (reactants and cycloadducts) using the second order González–Schlegel integration method.[32] Thermochemical properties (enthalpy, entropy, and Gibbs free energy) were calculated according to the standard equations of statistical thermodynamics[33] at 298.15 K. For the thermochemical evaluation, theoretical calculations are performed with the Truhlar's MPW1B95 density functional,[20] together with the standard 6-31G(d) basis set. The electronic structures of stationary points were analysed by the natural bond orbital (NBO) method[34] and the topological analysis of the electron localization function (ELF), η(r).[25,35] The ELF study was performed with the TopMod program.[36] Solvent effects have been considered at the same level of theory by geometry single point of the gas-phase structures

using a self-consistent reaction field (SCRF)[37] based on the continuum salvation model (SMD) of the Truhlar's group.[38] Since this cycloaddition is carried out in DCM, we have selected its dielectric constant at 298.0 K, ε=8.93. The global electrophilicity index, ω,[39] which measures the stabilization energy when the system acquires an additional electronic charge ΔN from the environment, has been given by the following simple expression, $\omega = (\mu^2 / 2\eta)$,[39] in terms of the electronic chemical potential μ and the chemical hardness η. Both quantities may be approached in terms of the one electron energies of the frontier molecular orbital HOMO, ε_H, and LUMO, ε_L, as $\mu \approx (\varepsilon_H + \varepsilon_L)/2$ and $\eta \approx (\varepsilon_L - \varepsilon_H)$, respectively.[40] The reactivity indices were computed from the B3LYP/6-31G(d) HOMO and LUMO energies at the ground state of the reactants.

Acknowledgements

Financial support from the Ministry of Higher Education and Scientific Research of the Algerian Government (project CNEPRU E02020110003) is gratefully acknowledged.

References

1 A. Padwa, W. H. Pearson, *The Chemistry of Heterocyclic Compounds, Synthetic Applications of 1,3-Dipolar Cycloaddition Chemistry Toward Heterocycles and Natural Products*, John Wiley & Sons, 2002.

2 (*a*) P. Merino, T. Tejero, F. J. Unzurrunzaga, S. Franco, U. Chiacchio, M. G. Saita, D. Iannazzo, A. Piperno, G. Romeo, *Tetrahedron:Asymmetry*, 2005, **16**, 3865; (*b*) V. Mannucci, F. M. Cordero, A. Piperno, G. Romeo, A. Brandi, *Tetrahedron:Asymmetry*, 2008, **19**, 1204; (*c*) R. Romeo, S. V. Giofre, B. Macchi, E. Balestrieri, A. Mastino, P. Merino, C. Carnovale, G. Romeo, U. Chiacchio, *Chem. Med. Chem.*, 2012, **7**, 565.

3 (*a*) T. Kiguchi, M. Shirakawa, R. Honda, I. Ninomiya, T. Naito, *Tetrahedron*, 1998, **54**, 15589; (*b*) F. Cardona, G. Moreno, F. Guarna, P. Vogel, C. Schuetz, P. Merino, A. Goti, *J. Org. Chem.*, 2005, **70**, 6552; (*c*) I. Delso, T. Tejero, A. Goti, P. Merino, *Tetrahedron*, 2010, **66**, 1220; (*d*) J. Peng, D. Jiang, W. Lin, Y. Chen, *Org. Biomol. Chem.*, 2007, **5**, 1391; (*e*) M. M. Andrade, M. T. Barros, R. C. Pinto, *Clean and Sustainable Methodologies for the Synthesis of Isoxazolidines*. In *Heterocyclic Targets*

in Advanced Organic Synthesis; M. C. Carreiras, Marco-Contelles J. Eds Research Signpost:Trivandrum, 2002, **51**, 67.

4 T. Saito, T. Yamada, S. Miyazaki, T. Otani, *Tetrahedron Lett.*, 2004, **45**, 9585.

5 K. V. Gothelf, K. V. Jørgensen, *Chem. Rev.* 1998, **98**, 863.

6 R. B. Woodward, R. Hoffmann, *The Conservation of Orbital Symmetry, Verlag Chemie*: Weinheim, 1970.

7 (*a*) D. Carmona, M. P. Lamata, F. Viguri, R. Rodriguez, L. A. Oro, F. J. Lahoz, A. I. Balana, T. Tejero, P. Merino, *J. Am. Chem. Soc.*, 2005, **127**, 13386 ; (*b*) D. Carmona, M. P. Lamata, F. Viguri, J. Ferrer, N. Garcia, F. J. Lahoz, M. L. Martin, L. A. Oro, *Eur. J. Inorg. Chem.*, 2006, 3155 ; (*c*) D. Carmona, M. P. Lamata, F. Viguri, R. Rodriguez, F. J. Lahoz, L. A. Oro, *Chem. Eur. J.*, 2007, **13**, 9746 ; (*d*) T. Hashimoto, M. Omote, Y. Hato, T. Kano, K. Maruoka, *Chem. Asian. J.*, 2008, **3**, 407; (*e*) D. Carmona, M. P. Lamata, F. Viguri, R. Rodriguez, F. J. Lahoz, M. J. Fabra, L. A. Oro, *Tetrahedron: Asymmetry*, 2009, **20**, 1197; (*f*) M. Lemay, J. Trant, W. W. Ogilvie, *Tetrahedron*, 2007, **63**, 11644; (*g*) S. S. Chow, M. Nevalainen, C. A. Evans, C. W. Johannes, *Tetrahedron Lett.*, 2007, **48**, 277.

8 (*a*) M. Frederickson, *Tetrahedron*, 1997, **5**, 403; (*b*) S. Karlsson, H. E. Högberg, *Org. Prep. Proced. Int.*, 2001, **33**, 103; (*c*) T. B. Nguyen, A. Martel, C. Gaulon, R. Dhal, G. Dujardin, *Organic Preparations and Procedures International*, 2010, **42**, 387; (*d*) H. Pellissier, *Tetrahedron*, 2012, **68**, 2197; (*e*) Y. Xing, N. Wang, *Coordination Chemistry Reviews*, 2012, **256**, 938; (*f*) W. Wang, K. S. Rein, *Tetrahedron Letters*, 2013, **54**, 1866.

9 V. Bãdoiu, E. P. Kündig, *Org. Biomol. Chem.*, 2012, **10**, 114.

10 (*a*) K. V. Gothelf, R. G. Hazell, K. A. Jørgensen, *J. Org. Chem.*, 1996, **61**, 346; (*b*) P. Merino, J. Revuelta, T. Tejero, U. Chiacchio, A. Rescifinab, G. Romeo, *Tetrahedron*, 2003, **59**, 3581; (*c*) P. Astolfi, P. Bruni, L. Greci, P. Stipa, L. Righi, C. Rizzoli, *Eur. J. Org. Chem.*, 2003, 2626 ; (*d*) C. T. Wong, *Tetrahedron*, 2013, **69**, 6634.

11 N. Acharjeea, T. K. Das, A. Banerji, M. Banerjee, T. Prangé, *J. Phys. Org. Chem.*, 2010, **23**, 1187.

12 M. Flores, P. García, N. M. Garrido, C. T. Nieto, P. Basabe, I. S. Marcos, F. Sanz-González, J. M. Goodman, D. Díez, *Tetrahedron: Asymmetry*, 2012, **23**, 76.

13 M. Śnieżek, S. Stecko, I. Panfil, B. Furman, Z. Urbańczyk-Lipkowska, M. Chmielewski, *Tetrahedron: Asymmetry*, 2013, **24**, 89.

14 L. R. Domingo, W. Benchouk, S. M. Mekelleche, *Tetrahedron*, 2007, **63**, 4464.

15 W. Benchouk, S. M. Mekelleche, *J. of Mol. Struct.: THEOCHEM*, 2008, **852**, 46.

16 J. Liu, S. Niwayama, Y. You, K. N. Houk, *J. Org. Chem.,* 1998, **63***,* 1064.

17 C. Barba, D. Carmona, J. I. García, M. P. Lamata, J. A. Mayoral, L. Salvatella, F. Viguri, *J. Org. Chem.*, 2006, **71**, 9831.

18 C. Reichardt, T. Welton, *Solvents and Solvent Effects in Organic Chemistry*, (4th Edition), Wiley-VCH, 2011.

19 W. Benchouk, S. M. Mekelleche, B. Silvi, M. J. Aurell, L. R. Domingo, *J. Phys. Org. Chem.*, 2011, **24**, 611.

20 Y. Zhao, D. G. Truhlar, *J. Phys. Chem. A*, 2004, **108**, 6908.

21 (*a*) A. Shiroudi, E. Zahedi, *Progress in Reaction Kinetics and Mechanism*, 2012, **37**, 277; (*b*) L. R. Domingo, P. Pérez, J. A. Sáez, *RSC Adv*, 2013, **3**, 7520.

22 C. Y. Legault, CYLView, 1.0b, Université de Sherbrooke, Canada, 2009 http://www.cylview.org.

23 K. B. Wiberg, *Tetrahedron*, 1968, **24**, 1083.

24 (*a*) S. Berski, J. Andres, B. Silvi, L. R. Domingo, *J. Phys. Chem. A*, 2006, **110**, 13939; (*b*) V. Polo, J. Andres, S. Berski, L. R. Domingo, B. Silvi, *J. Phys. Chem. A*, 2008, **112**, 7128; (*c*) W. Benchouk, S. M. Mekelleche, M. J. Aurell, L. R. Domingo, *Tetrahedron*, 2009, **65**, 4644; (*d*) L. R. Domingo, E. Chamorro, P. Pérez, *Org. Biomol. Chem.*, 2010, **8**, 5495; (*e*) L. R. Domingo, P. Pérez, J. A. Sáez, *Org. Biomol. Chem.*, 2012, **10**, 3841 ; (*f*) L. R. Domingo, P. Pérez, J. A. Sáez, *Tetrahedron*, 2013, **69**, 107 ; (*g*) L. Rhyman, P. Ramasami, J. A. Joule, J. A. Sáez, L. R. Domingo, *RSC Adv.*, 2013, **3**, 447 ; (*h*) L. R. Domingo, P. Pérez, J. A. Sáez, *Org. Biomol. Chem.*, 2013, **11**, 4350; (*i*) L. R. Domingo, J. A. Sáez, J. A. Joule, L. Rhyman, P. Ramasami, *J. Org. Chem.*, 2013, **78**, 1621.

25 B. Silvi, *J. Mol. Struct.*, 2002, **614**, 3

26 L. R. Domingo, M. J. Aurell, P. Perez, R. Contreras, *Tetrahedron*, 2002, **58**, 4417.

27 Gaussian 09, Revision A.1, M. J. Frisch, G. W. Trucks, H. B. Schlegel, G. E. Scuseria, M. A. Robb, J. R. Cheeseman, G. Scalmani, V. Barone, B. Mennucci, G. A. Petersson, H. Nakatsuji, M. Caricato, X. Li, H. P. Hratchian, A. F. Izmaylov, J. Bloino, G.

Zheng, J. L. Sonnenberg, M. Hada, M. Ehara, K. Toyota, R. Fukuda, J. Hasegawa, M. Ishida, T. Nakajima, Y. Honda, O. Kitao, H. Nakai, T. Vreven, J. A. Montgomery, Jr., J. E. Peralta, F. Ogliaro, M. Bearpark, J. J. Heyd, E. Brothers, K. N. Kudin, V. N. Staroverov, R. Kobayashi, J. Normand, K. Raghavachari, A. Rendell, J. C. Burant, S. S. Iyengar, J. Tomasi, M. Cossi, N. Rega, J. M. Millam, M. Klene, J. E. Knox, J. B. Cross, V. Bakken, C. Adamo, J. Jaramillo, R. Gomperts, R. E. Stratmann, O. Yazyev, A. J. Austin, R. Cammi, C. Pomelli, V. Ochterski, R. L. Martin, K. Morokuma, V. G. Zakrzewski, G. A. Voth, P. Salvador, J. J. Dannenberg, S. Dapprich, A. D. Daniels, Ö. Farkas, J. B. Foresman, J. V. Ortiz, J. Cioslowski and D. J. Fox, Gaussian, Inc., Wallingford CT, 2009.

28 (*a*) A. D. Becke, *J. Chem. Phys.*, 1993, **98**, 5648; (*b*) C. Lee, W. Yang, R. G. Parr, *Phys. Rev. B*, 1988, **37**, 785.

29 W. J. Hehre, L. Radom, Pv. R. Schleyer, J. A. Pople, *Ab Initio Molecular Orbital Theory*, Wiley, 1986.

30 (*a*) H. B. Schlegel, *J. Comput. Chem.*, 1982, **3**, 214; (*b*) H. B. Schlegel, *Geometry Optimization on Potential Energy Surface. In Modern Electronic Structure Theory*, D. R. Yarkony Ed. World Scientific Publishing, 1994.

31 K. J. Fukui, *Phys. Chem.*, 1970, **74**, 4161.

32 (*a*) C. González, H. B. Schlegel, *J. Phys. Chem.*, 1990, **94**, 5523; (*b*) C. González, H. B. Schlegel, *J. Chem. Phys.*, 1991, **95**, 5853.

33 C. J. Cramer, *Essentials of Computational Chemistry Theories and Models*, Wiley Hoboken, 2004.

34 (*a*) A. E. Reed, L. A. Curtiss, F. Weinhold, *Chem. Rev.*, 1988, **88**, 899; (*b*) A. E. Reed, R. B. Weinstock, F. Weinhold, *J. Chem. Phys.*, 1985, **83**, 735.

35 (*a*) A. Savin, A. D. Becke, J. Flad, R. Nesper, H. Preuss, H. G. Vonschnering, *Angew Chem. Int. Ed. Engl.*, 1991, **30**, 409; (*b*) B. Silvi, A. Savin, *Nature*, 1994, **371**, 683; (*c*) A. Savin, B. Silvi, F. Colonna, *Can. J. Chem.*, 1996, **74**, 1088; (*d*) A. Savin, R. Nesper, S. Wengert, T. F. Fassler, *Angew Chem. Int. Ed.*, 1997, **36**, 1808.

36 S. Noury, X. Krokidis, F. Fuster, B. Silvi, *Comput. Chem.*, 1999, **23**, 597.

37 (*a*) J. Tomasi, M. Persico, Chem. Rev., 1994, **94**, 2027; (*b*) B. Y. Simkin, I. Sheikhet, *Quantum Chemical and Statistical Theory of Solutions-A Computational Approach*, Ellis Horwood, 1995.

38 (*a*) A. V. Marenich, C. J. Cramer, D. G. Truhlar, *J. Phys. Chem. B*, 2009, **113**, 6378; (*b*) R. F. Ribeiro, A. V. Marenich, C. J. Cramer, D. G. Truhlar, *J. Phys. Chem. B*, 2011, **115**, 14556.

39 R. G. Parr, L. von Szentpaly, S. J. Liu, *Am. Chem. Soc.*, 1999, **121**, 1922.

40 (*a*) R. G. Parr, R. G. Pearson, *J. Am. Chem. Soc.*, 1983, **105**, 7512; (*b*) R. G. Parr, W. Yang, *Density Functional Theory of Atoms and Molecules, Oxford University Press*, 1989.

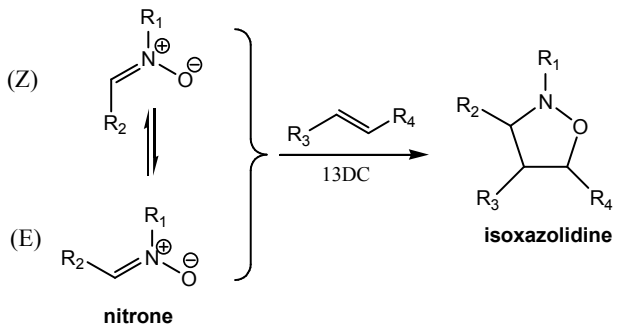

Scheme 1

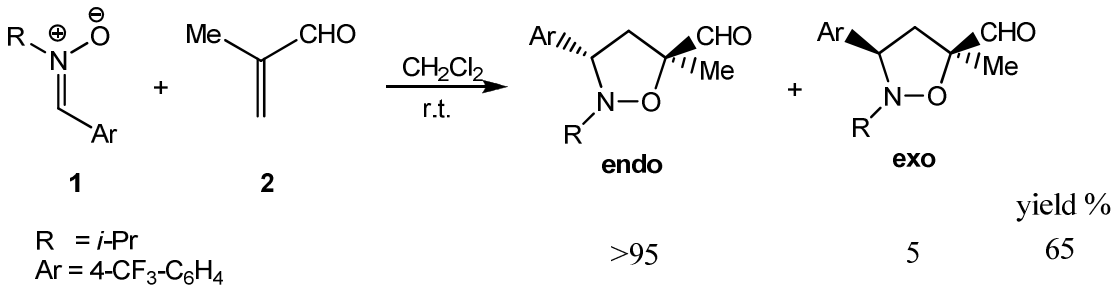

			yield %
R = *i*-Pr Ar = 4-CF_3-C_6H_4	>95	5	65

Scheme 2

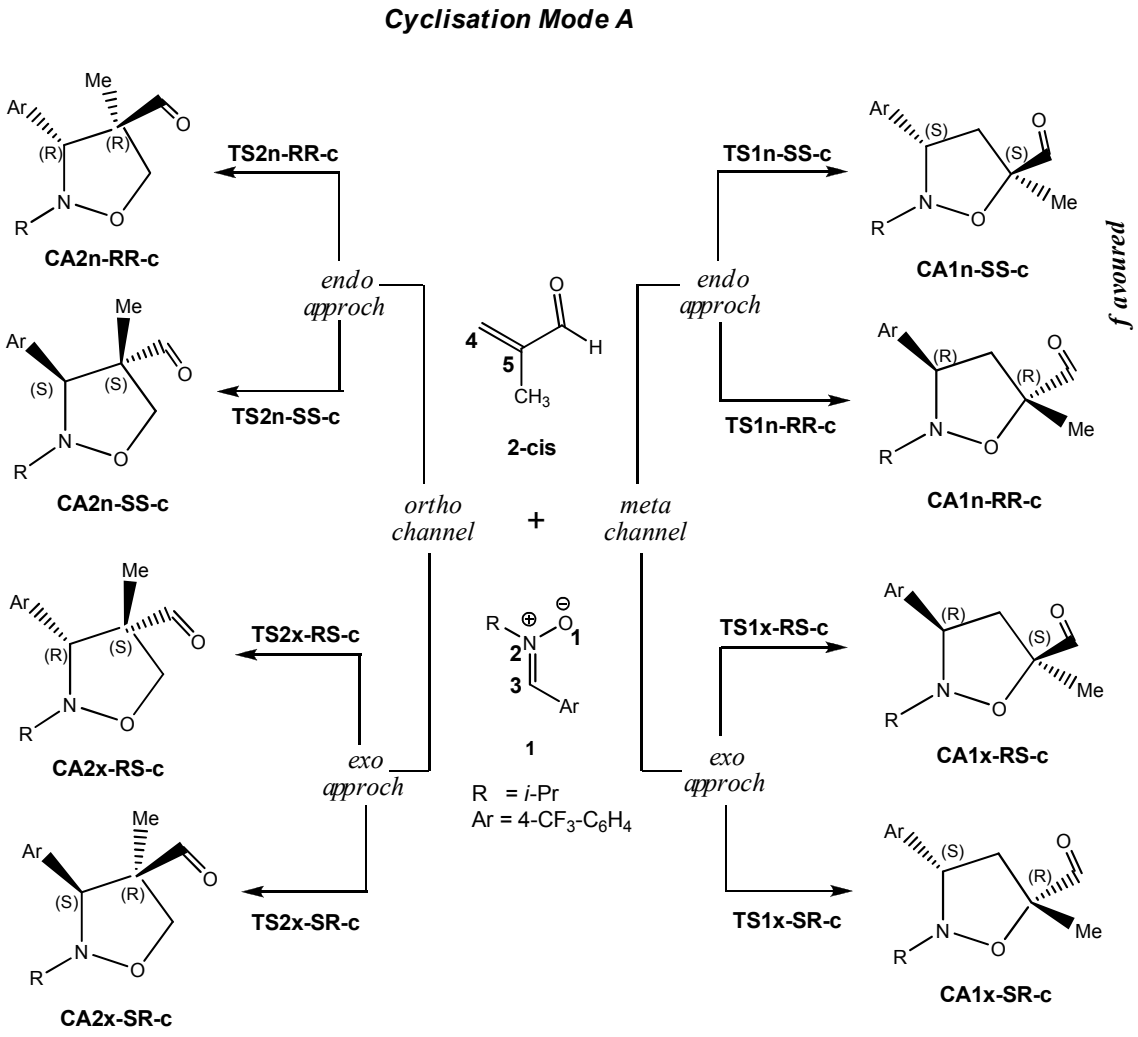

Scheme 3: Regio- and stereoisomeric channels corresponding to the 13DC reaction of α-arylnitrone **1** with methacrolein **2-cis.**

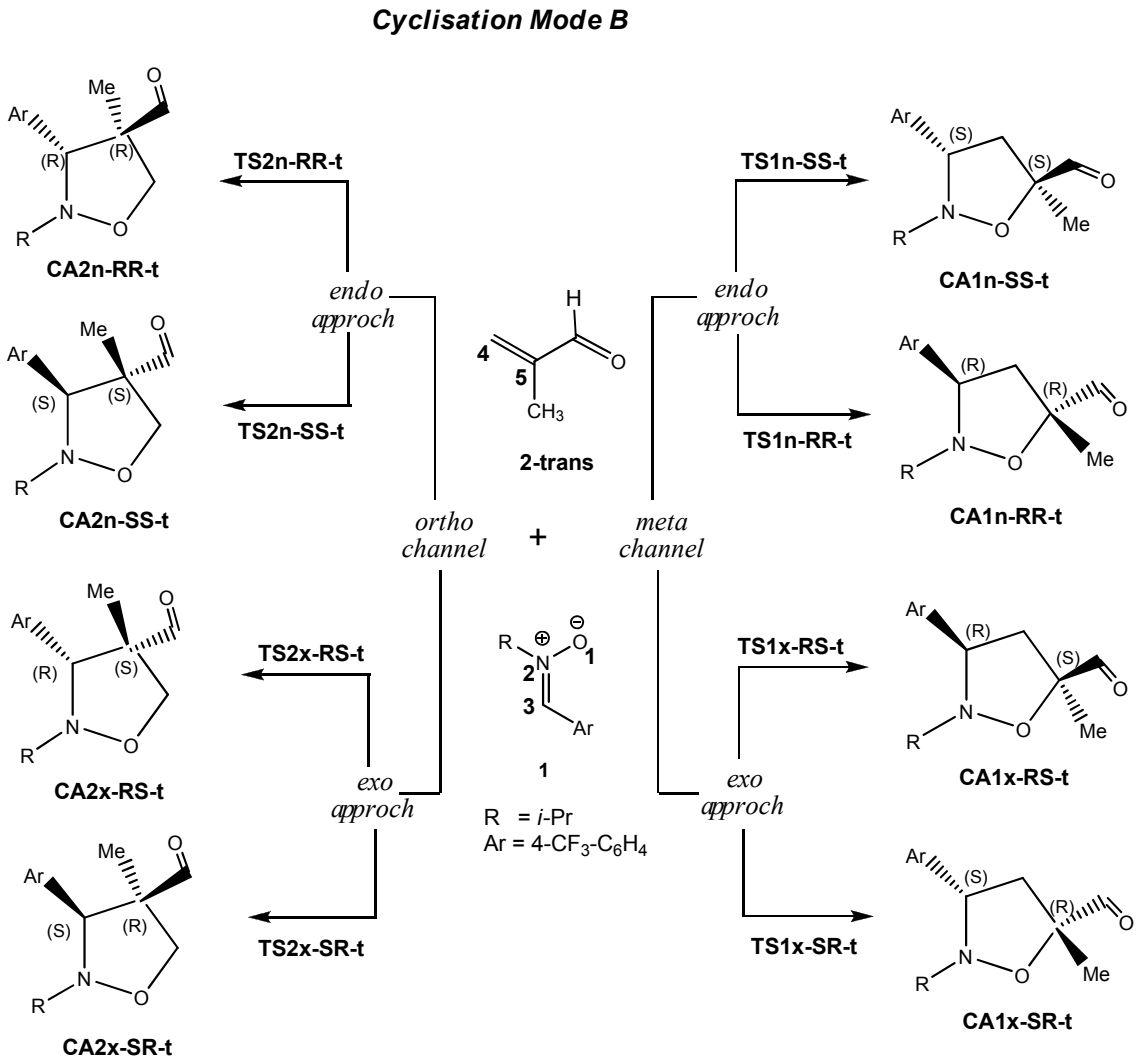

Scheme 4: Regio- and stereoisomeric channels corresponding to the 13DC reaction of α-arylnitrone **1** with methacrolein **2-trans.**

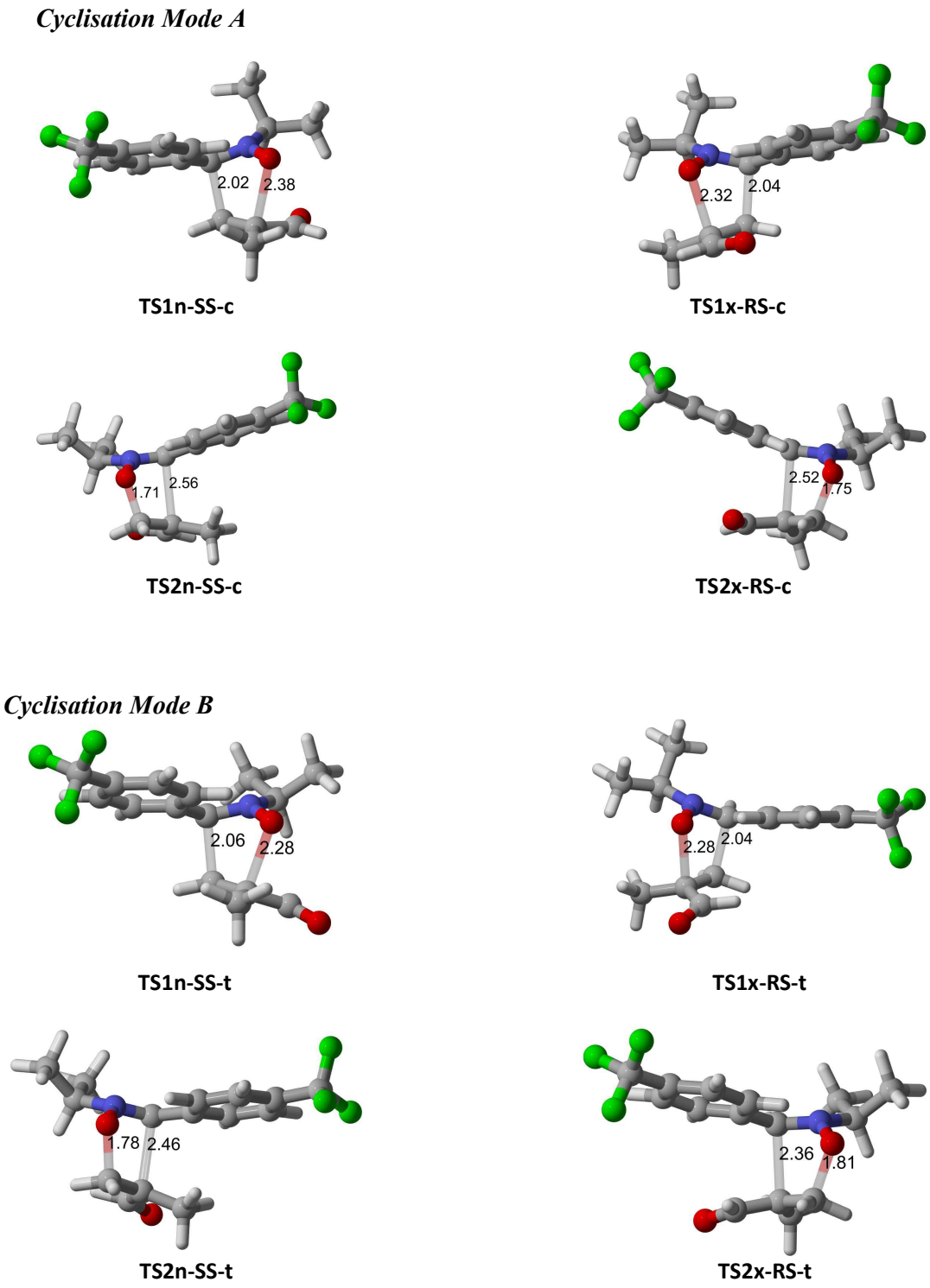

Figure 1: B3LYP/6-31G(d) geometries of the transition structures involved in the 13DC reaction between the α-aryl nitrone **1** and methacrolein **2** via **CM-A** and **CM-B**. Lengths are given in Angstroms.

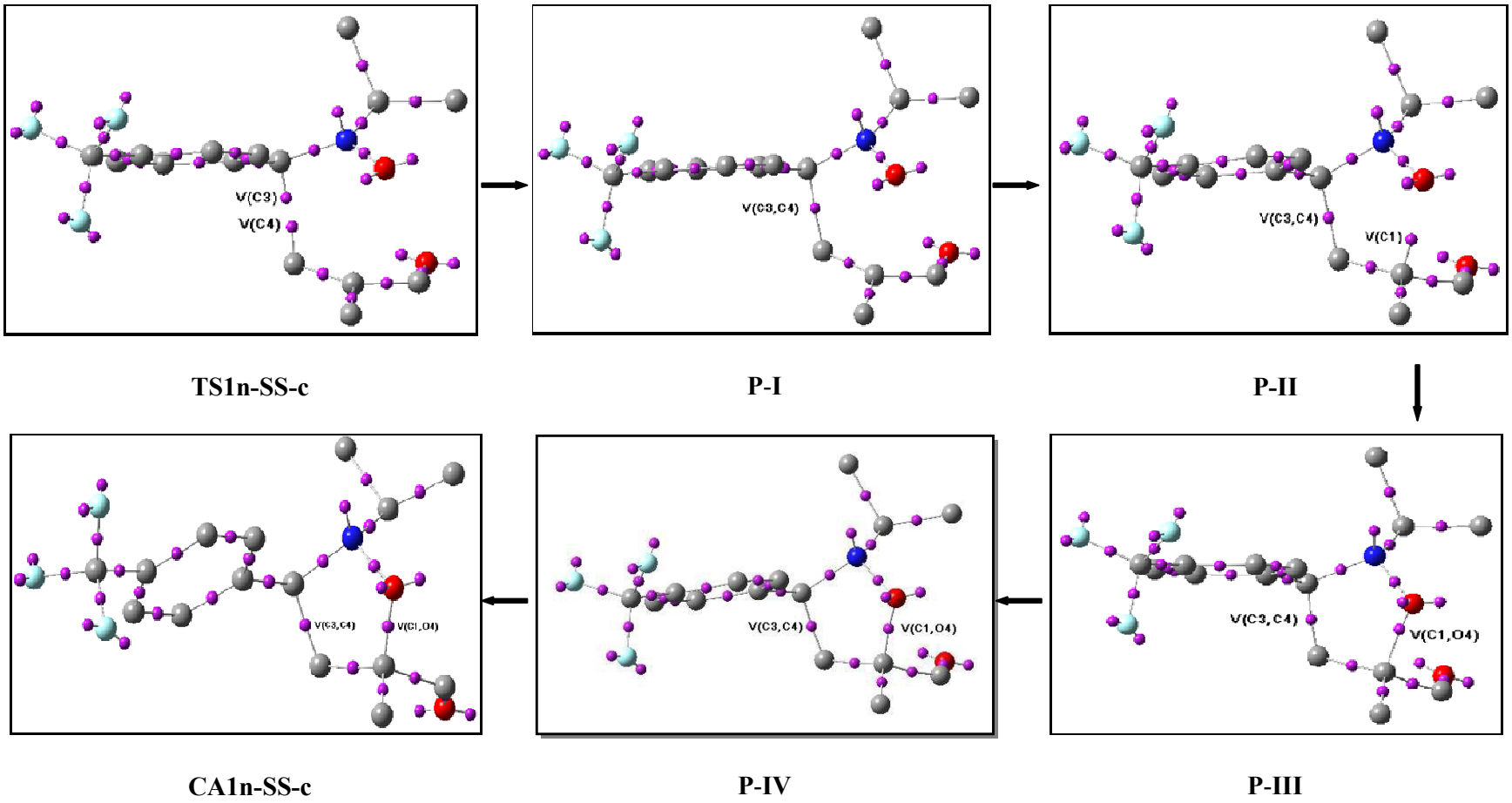

Figure 2: Schematic representation of the mono- and disynaptic ELF basins for some relevant points on the IRC curve of the *meta-endo* channel via **CM-A**. The hydrogen atoms are omitted for clarity.

Table 1. Total (E, in a.u.) and relative[a] (ΔE, in kcal/mol) B3LYP/6-31G(d) energies in gas phase and in DCM for the 13DC reaction of the α-aryl nitrone **1** and methacrolein **2-cis/trans**.

	gas phase		dichloromethane	
	E	ΔE[a]	E	ΔE[a]
Cyclisation Mode A				
1	-855.852632		-855.868923	
2-cis	-231.228858		-231.235911	
TS1n-SS-c	-1087.056973	15.4	-1087.075835	18.2
TS1n-RR-c	-1087.056973	15.4	-1087.075835	18.2
TS1x-RS-c	-1087.047561	21.3	-1087.068575	22.8
TS1x-SR-c	-1087.047561	21.3	-1087.068575	22.8
TS2n-RR-c	-1087.054962	16.6	-1087.072847	20.1
TS2n-SS-c	-1087.054962	16.6	-1087.072847	20.1
TS2x-RS-c	-1087.045425	22.6	-1087.066997	23.7
TS2x-SR-c	-1087.045425	22.6	-1087.066997	23.7
CA1n-SS-c	-1087.103057	-13.5	-1087.121751	-10.6
CA1n-RR-c	-1087.103057	-13.5	-1087.121751	-10.6
CA1x-RS-c	-1087.101302	-12.4	-1087.120545	-9.9
CA1x-SR-c	-1087.101302	-12.4	-1087.120547	-9.9
CA2n-RR-c	-1087.093715	-7.7	-1087.112313	-4.7
CA2n-SS-c	-1087.093715	-7.7	-1087.112313	-4.7
CA2x-RS-c	-1087.093189	-7.3	-1087.112755	-5.0
CA2x-SR-c	-1087.093189	-7.3	-1087.112755	-5.0
Cyclisation Mode B				
1	-855.852632		-855.868923	
2-trans	-231.233543		-231.240636	
TS1n-SS-t	-1087.053972	20.2	-1087.075862	21.1
TS1n-RR-t	-1087.053972	20.2	-1087.075862	21.1
TS1x-RS-t	-1087.049825	22.8	-1087.071497	23.9
TS1x-SR-t	-1087.049825	22.8	-1087.071498	23.9
TS2n-RR-t	-1087.051335	21.9	-1087.072337	23.4
TS2n-SS-t	-1087.051335	21.9	-1087.072337	23.4
TS2x-RS-t	-1087.048214	23.8	-1087.069159	25.4
TS2x-SR-t	-1087.048214	23.8	-1087.069159	25.4
CA1n-SS-t	-1087.101744	-9.8	-1087.121365	-7.4
CA1n-RR-t	-1087.101744	-9.8	-1087.121365	-7.4
CA1x-RS-t	-1087.101181	-9.4	-1087.121480	-7.5
CA1x-SR-t	-1087.101181	-9.4	-1087.121479	-7.5
CA2n-RR-t	-1087.095235	-5.7	-1087.114731	-3.2
CA2n-SS-t	-1087.095235	-5.7	-1087.114732	-3.2
CA2x-RS-t	-1087.094966	-5.5	-1087.114233	-2.9
CA2x-SR-t	-1087.094966	-5.5	-1087.114233	-2.9

[a] Relative to reactants

Table 2. MPW1B95/6-31G(d) thermodynamic data, in DCM and at 25 °C, for the 13DC reaction of the α-aryl nitrone **1** and methacrolein **2-cis/trans**.

	H a.u.	ΔH[a] Kcal/mol	S cal/K.mol	ΔS[a] cal/K.mol	G a.u.	ΔG[a] Kcal/mol
Cyclisation Mode A						
1	-855.309925		118.9		-855.366395	
2-cis	-231.019909		73.3		-231.054730	
TS1n-SS-c	-1086.307791	13.8	144.0	-48.2	-1086.376193	28.2
TS1n-RR-c	-1086.307791	13.8	144.0	-48.2	-1086.376193	28.2
TS1x-RS-c	-1086.301136	18.0	141.5	-50.6	-1086.368381	33.1
TS1x-SR-c	-1086.301136	18.0	141.5	-50.6	-1086.368381	33.1
TS2n-RR-c	-1086.306374	14.7	142.7	-49.5	-1086.374158	29.5
TS2n-SS-c	-1086.306374	14.7	142.7	-49.5	-1086.374158	29.5
TS2x-RS-c	-1086.300008	18.7	144.4	-47.8	-1086.368599	33.0
TS2x-SR-c	-1086.300009	18.7	144.4	-47.8	-1086.368598	33.0
CA1n-SS-c	-1086.360914	-19.5	141.4	-50.7	-1086.428111	-4.4
CA1n-RR-c	-1086.360914	-19.5	141.4	-50.7	-1086.428111	-4.4
CA1x-RS-c	-1086.360058	-19.0	142.5	-49.7	-1086.427743	-4.2
CA1x-SR-c	-1086.360054	-19.0	142.4	-49.7	-1086.427720	-4.1
CA2n-RR-c	-1086.352762	-14.4	142.5	-49.6	-1086.420486	0.4
CA2n-SS-c	-1086.352762	-14.4	142.5	-49.6	-1086.420486	0.4
CA2x-RS-c	-1086.353005	-14.5	141.6	-50.5	-1086.420301	0.5
CA2x-SR-c	-1086.353005	-14.5	141.6	-50.5	-1086.420301	0.5
Cyclisation Mode B						
1	-855.309925		118.9		-855.366395	
2-trans	-231.024436		72.6		-231.058921	
TS1n-SS-t	-1086.307338	17.0	145.4	-46.0	-1086.376416	30.7
TS1n-RR-t	-1086.307339	17.0	145.4	-46.0	-1086.376420	30.7
TS1x-RS-t	-1086.303120	19.6	145.8	-45.6	-1086.372417	33.2
TS1x-SR-t	-1086.303120	19.6	145.7	-45.7	-1086.372359	33.2
TS2n-RR-t	-1086.305426	18.2	145.3	-46.2	-1086.374444	31.9
TS2n-SS-t	-1086.305427	18.2	145.3	-46.2	-1086.374446	31.9
TS2x-RS-t	-1086.302206	20.2	144.5	-46.9	-1086.370860	34.2
TS2x-SR-t	-1086.302206	20.2	144.5	-46.9	-1086.370861	34.2
CA1n-SS-t	-1086.360931	-16.7	142.6	-48.8	-1086.42870	-2.1
CA1n-RR-t	-1086.360931	-16.7	142.6	-48.8	-1086.428705	-2.1
CA1x-RS-t	-1086.359664	-15.9	144.7	-46.8	-1086.428399	-1.9
CA1x-SR-t	-1086.359665	-15.9	144.7	-46.8	-1086.428402	-1.9
CA2n-RR-t	-1086.355063	-13.0	141.1	-50.3	-1086.422120	2.0
CA2n-SS-t	-1086.355062	-13.0	141.1	-50.3	-1086.422114	2.0
CA2x-RS-t	-1086.355060	-13.0	142.6	-48.9	-1086.422801	1.6
CA2x-SR-t	-1086.355060	-13.0	142.6	-48.9	-1086.422801	1.6

[a] Relative to reactants

Table 3. Bond lengths, NBO bond orders (BO) and valence basin populations N (calculated from the ELF analysis) of some selected points of the IRC curve of the favoured *meta-endo* reaction channel via **CM-A** between the α-aryl nitrone **1** and methacrolein **2-cis**.

		TS1n-SS-c	**P-I**	**P-II**	**P-III**	**P-IV**	**CA1n-SS-c**
d (Å)	C3—C4	2.02	1.70	1.61	1.57	1.56	1.55
	O1—C5	2.38	2.18	1.88	1.58	1.50	1.47
BO	C3—C4	0.48	0.81	0.90	0.95	0.96	0.97
	O1—C5	0.21	0.38	0.58	0.79	0.83	0.87
***N*(e)**	V(C3,C4)	—	1.58	1.73	1.80	1.83	1.85
	V(O1,C5)	—	—	—	0.92	1.09	1.19

Table 4. HOMO and LUMO energies (in a.u.), electronic chemical potential, μ (in a.u.), chemical hardness, η (in a.u.) and global electrophilicity, ω (in eV) for the reactants α-aryl nitrone **1** and methacrolein **2-cis**.

	ε_H	ε_L	μ	η	ω
1	-0.2154	-0.0624	-0.1389	0.1530	1.70
2-cis	-0.2551	-0.0611	-0.1581	0.1941	1.75